The Assembling of Semiconductor Nanocrystals

Alexey Shavel,[a] Nikolai Gaponik,[a,b] and Alexander Eychmüller*[a,b]

Keywords: Nanostructures / Colloids / Layer-by-layer assembly / Interactions

Recent accomplishments in arranging semiconductor nanoparticles in a desired manner are reviewed. Coupling mechanisms utilized for this purpose include electrostatic and covalent interactions, methods like layer-by-layer assembly, solvent-controlled precipitation and surface amination for covalent attachment of nanoparticles are employed. Dipole–dipole interactions are operative in nanocrystal solids and fast Förster energy transfer is observed.

Introduction

Ordered assemblies of nanocrystalline materials have received increasing interest in recent years. Nanoparticles (often referred to as artificial atoms) are used to build up artificial molecules and solids.[1] These arrays and superlattices offer new perspectives for the application of nanoparticles for example in optoelectronic devices. Various approaches toward assembling nanocrystals are known. Three-dimensional superlattices of semiconductor nanoparticles have been built up via self organization[2] and crystallization.[3–5] Another main route towards ordered structures of nanocrystals is covalent binding with and without special linker molecules.[6] These efforts have a direct correlation with the investigations in the fields of covalent coupling of nanoparticles to biomolecules and surface

[a] Institute of Physical Chemistry, University of Hamburg, Grindelallee 117, 20146 Hamburg, Germany
Fax: +49-351-46337164
E-mail: alexander.eychmueller@chemie.tu-dresden.de
[b] Institute of Physical Chemistry and Electrochemistry, Technical University of Dresden, Bergstraße 66b, 01062 Dresden, Germany

Alexander Eychmüller studied physics at the University of Göttingen. In 1987 he obtained his Ph. D., working on proton transfer reactions under the supervision of Dr. K.-H. Grellmann and Prof. A. Weller at the Max Planck Institute for Biophysical Chemistry. After a postdoctoral year at UCLA working with Prof. M. A. El-Sayed on gas phase metal clusters he joined the group of Prof. A. Henglein at the Hahn-Meitner-Institute in Berlin where he became involved in the research on semiconductor quantum dots. In 1994 he moved with Prof. H. Weller to the University of Hamburg focusing his scientific interests on the photophysical and structural properties of semiconductor nanocrystals. The habilitation in 1999 and the venia legendi in 2000 were followed by an offer of a chair in Physical Chemistry and Electrochemistry at the Technical University of Dresden in 2005.

Alexey Shavel was born in 1974 in Vitebsk, Belarus. He studied chemistry at the Belarusian State University from 1991 until 1996. From 1996 to 2002 he worked in the National Academy of Science of Belarus as a junior research scientist. In 2002 he started to work on his Ph. D. under the guidance of Dr. Alexander Eychmüller on the preparation of the nanoparticle superstructures.

Nikolai Gaponik studied chemistry and obtained his Ph. D. (2000) at the Belarusian State University working under the supervision of Prof. D. V. Sviridov on the electrochemical and photoelectrochemical properties of the composite materials based on conducting polymers and semiconductor nanocrystals. He worked as a visiting scientist at the LMU Munich with Dr. M. Gao and Prof. J. Feldmann in 2000. In October 2000 he joined the group of Prof. H. Weller and Dr. A. Eychmüller at the University of Hamburg first as a DAAD-fellow and finally as a research scientist. His current research interest focuses on the synthesis, characterization and applications of semiconductor nanocrystals.

MICROREVIEWS: This feature introduces the readers to the authors' research through a concise overview of the selected topic. Reference to important work from others in the field is included.

functionalization of nanocrystals.[7] Here we report on recent advances made in our Hamburg group in the preparation and the characterization of various assemblies of II-VI semiconductor nanocrystals (SC NCs). We will outline our efforts in the layer-by-layer assembling of SC NCs with and without interfacial polyelectrolytes. This method has been used to coat flat and porous solids as well as spherical microbeads. The latter may also be plated by solvent controlled precipitation of SC NCs onto them as will be shown in the subsequent paragraph. This will be followed by a survey of our experimental work devoted to the covalent coupling of nanoparticles amongst them as well as to flat and curved surfaces. The article will be finalized with a summary of our current theoretical understanding about the interparticle interactions and a kinetic study of Förster energy transfer in SC NC solids.

Layer-by-layer Assembly of Semiconductor Nanocrystals

LbL Assembly on Flat and/or Porous Surfaces

Uniform and multicomponent thin films consisting of functional molecules and/or nanocrystals may be formed by applying the so-called layer-by-layer (LbL) assembly technique. Figure 1 shows, schematically, the LbL procedure which was originally introduced for the assembly of polymer electrolytes[8] and, which was recently adapted to the deposition of charged nanocrystals both on flat[9,10] and on curved surfaces.[11,12] As is seen from Figure 1 the formation of monolayers of deposited material is based on the electrostatic interaction between the nanocrystals and the surface. Alternation of the sign of the charges of the species to be deposited allows the multilayers to grow quite thick, while the introduction of new components in one of the layers yields the opportunity of virtually nonlimited but controllable variations of LbL-multistructure compositions.[13,14] The application of the method described to the modification of artificial opals yielded intrinsically light emitting photonic crystals, which were successfully used for investigations on photonic confinement phenomena.[15,16]

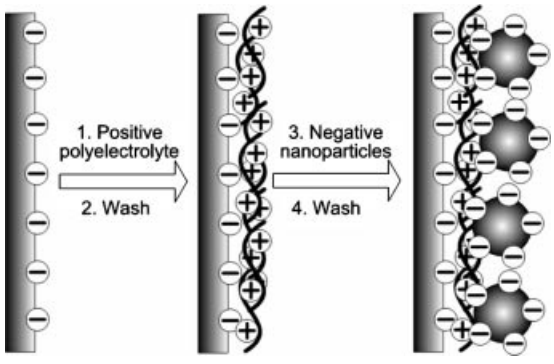

Figure 1. Schematic representation of the LbL assembly involving polyelectrolyte molecules and oppositely charged nanoparticles. The procedures 1–4 can be repeated to assemble more PE/nanoparticles bilayers.

The following standard cyclic procedure is normally used for the preparation of layered structures of negatively charged nanocrystals: (i) dipping of the substrate into a solution of polyelectrolyte (PE) (e.g. 5 mg ml^{-1} in 0.5 M NaCl) for 10 min [poly(ethyleneimine), PEI, was used for the first layer and poly(diallyldimethylammonium chloride), PDDA, for the second and further layers]; (ii) rinsing with water for 1 min; (iii) dipping into aqueous dispersions of the nanocrystals for 20 min; (iv) rinsing with water again for 1 min (cf. Figure 1). On each of the exposed surfaces, this procedure results in a 'bilayer' consisting of a polymer/NC composite. The cycle can be repeated as many times as necessary to obtain a multilayer film of desired thickness. The thickness of the LbL film depends linearly on the number of 'bilayers'. Moreover, a linear dependence of the absorption in the region of the first absorption maximum on the number of bilayers was observed.[17,18]

It is mentioned that in some cases the LbL assembly appeared to be nonefficient. When using freshly prepared colloidal solutions of nanocrystals we occasionally observed incomplete layer formation. Low-molecular weight byproducts of the synthesis as well as the smallest nanocrystal precursors could be responsible for this because they may be attracted by the polyelectrolyte sub-layers with higher efficiency than the nanocrystals themselves. We assume that aging of nanocrystal colloidal solutions leads to the reduction of the activity of those poisoning species due to their association with particle shells, aggregation and precipitation, etc. To avoid this problem, i.e. to make nanocrystal colloidal solutions useful for LbL assembly without aging them, we developed an electrophoretic activation of the colloidal solutions of thiol-capped nanocrystals. The nanocrystal solution that is to be activated is placed in a two-electrode electrochemical cell and a 1.5–2 V potential is applied to the cell. The commonly used electrodes are flat stainless steel or ITO-glass plates with a 1 cm^2 working surface and 5 mm gap in between. The current density drops from ca. 100–120 μA cm^{-2} in the very beginning down to 5–10 μA cm^{-2} after 1 h of this treatment. The above-mentioned byproducts, and possibly other charged species, are electrophoretically assembled or reacted at the electrodes and the thus cleaned activated solutions can be used for the LbL deposition as usual after removal from the cell.

Electrostatic Assembly of NCs

However, in these LbL systems the distance between donors and acceptors can not be shorter than the thickness of the polyelectrolyte monolayer. In order to avoid this limitation, which may be unfavorable for efficient interparticle interactions (see below), a new kind of a LbL structure has been generated.[19] The building blocks of the system were water soluble CdTe NCs with opposite surface charges (the charge of the CdTe NCs depends on the kind of stabilizer[20]), which were LbL assembled without polyelectrolytes between the particle layers. However, we encountered intrinsic limitations such as an easy removal of the already

deposited layers and the unbeneficial balance of charges during the film growth.[21] These limitations might have less influence in the case of the assembly of only one NC bilayer, while at the same time the inter-layer distance in this case would be further reduced leading to more efficient interactions. Bilayers of oppositely charged NCs can indeed be formed by a direct assembly of water-soluble CdTe NCs capped with amino- and carboxyl-group terminated short chain thiols. The preparation of this layered structure was performed in two steps. In the first step a polyelectrolyte sub-layer was formed followed by this standard procedure: (i) dipping of the substrate into PEI solution for 20 min; (ii) rinsing with water for 1 min; and (iii) dipping into poly-(sodium 4-styrene sulfonate) (PSS) solution (iv) and final rinsing in water. The first PEI layer was used to improve the quality of the layered structure in terms of uniform surface coverage.[10] In the second step, close-packed nanoparticle structures on the surface of the polyelectrolyte's bilayer were assembled as follows. The substrate with the PE bilayer was (i) dipped into aqueous dispersions of the 2-mercaptoethylamine (MA)-capped nanocrystals for 20 min, (ii) rinsed with water for 1 min and finally (iii) dipped into an aqueous dispersion of the mercaptopropionic acid (MPA)- or thioglycolic acid (TGA)-capped nanocrystals, again for 20 min. Such a procedure results in a layered structure consisting of a support/polymer/NCs-NCs composite. Typical absorption and photoluminescence spectra of the system are shown in Figure 2. The composite of the nanoparticles exhibits absorption only from the bottom layer of NCs (the absorption from the top NC layer is below the limit of the sensitivity of our spectrophotometer). At the same time emission associated mainly with the top layer is observed, which is taken as a first hint to efficient energy transfer (see below).

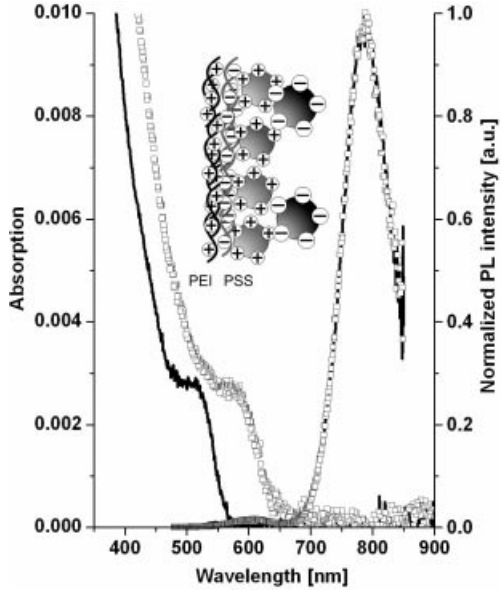

Figure 2. Examples of two close-packed structures utilizing MA-capped CdTe NCs (positively charged) of ca. 2 nm (black solid lines) and 4 nm (open squares) as the bottom layer. MPA-capped nanocrystals (negatively charged) of 6–8 nm in diameter were used as the top layer in both structures shown. While the absorption spectra of the structures show only the features corresponding to the bottom layer, the photoluminescence of the top layer (centered at ca. 780 nm) dominates in both structures.

LbL Assembly on Microbeads

The LbL assembly of NCs on the surface of the polymer [polystyrene, PMMA, melamineformaldehyde (MF) etc.] or silica beads opens up an opportunity to create submicro-sized objects exhibiting the properties of nanosized components.[22,23] In this case the LbL assembly can be done by suspension of the beads in solutions of the corresponding layer component. The contents of the solutions are generally the same as for the procedures described above. Repetitive centrifugations from pure water suspensions are used for washing of the beads and removal of excessive or nonspecifically adsorbed reactants. Figure 3 shows typical TEM images of the LbL modified beads. The modified beads retain the luminescence properties of the NCs used with a slight red shift of the luminescence maximum due to energy transfer from the smallest to the largest NCs in the assembled surface film.[11,24] The comparatively large size of the beads enables them to be manipulated by optical tweezers or to be used as a tip mounted at the end of an optical fiber. Thus, the beads can be used as subwavelength-sized light sources for photonic applications[25] or for the selective amplification of a signal in scanning near-field optical microscopy (SNOM).[26] The LbL modified beads of larger sizes (>2 μm) show an efficient coupling of the light emitted by the NCs with the whispering gallery modes of the spherical microresonators.[27–29] The use of beads made from materials that can be dissolved after LbL deposition of the polyelectrolytes (like e.g. MF, $MnCO_3$, etc.) allows the formation of hollow polyelectrolyte/NCs shells.[30–32] The shells are promising as microcapsules for drug delivery systems where the luminescence of inserted nanocrystals can be used for the monitoring of the delivery process.[33]

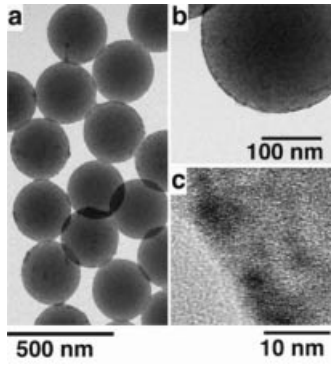

Figure 3. TEM and high-resolution TEM images of CdTe nanocrystals on polystyrene beads with increasing resolution from a) to c). The efficient coverage of the beads with nanocrystals is clearly seen in c) where the crystal structure of individual nanocrystals is resolved. Reproduced from ref.[26] with permission, copyright 2004 American Chemical Society.

Solvent-Controlled Precipitation

Another method of coating microspheres has been established through the controlled precipitation of nanocrystals by means of their aggregation in solution onto latex spheres.[34] The approach is a variation of heteroaggregation phenomena in a colloidal environment. The aggregation of NCs onto colloidal beads was induced by the solvent-nonsolvent pair precipitation technique which is normally successfully used to separate semiconductor nanocrystals by size. Colloidal cores statistically harvest aggregated nanocrystals, which consequently leads to the formation of a shell. Moreover, the thickness of the shell can efficiently be controlled through the proper choice of the concentration ratio of the colloidal particles serving as the cores and the precipitated species. Luminescent CdTe NCs were stabilized with TGA and thus exhibit a negatively charged surface, which was used to coat negatively charged sulfate stabilized polystyrene spheres, 468 nm in diameter. The latex spheres were precovered by an electrostatically adsorbed monolayer of positively charged polyallylamine hydrochloride (PAH). This modification was done in order to obtain a positively charged surface for better adhesion of the negatively charged NCs. Upon the addition of the NCs into the latex solution a monolayer of the NCs on the surface of the PS latex is formed due to the electrostatic interaction between the carboxylic groups of the NCs' stabilizer and the surface amino groups of the PAH-modified PS latex. The dropwise addition of ethanol (well known as "nonsolvent" for thiol-stabilized NCs[20]) to the latex NCs mixture initiates the aggregation of the NCs and allows for the creation of thicker shells on the beads. In the water/ethanol mixture (80% ethanol) the precipitation of the CdTe NCs on the latex spheres takes only minutes.

Alternatively, CdTe nanocrystals stabilized with MA, and thus being positively charged, were used for the solvent controlled precipitation by governing the pH of the solution. Earlier it has been demonstrated that these nanocrystals are stable and soluble in water in a pH region of 5.5–7 and tend to aggregate at higher pH values. Both, polystyrene and melamine formaldehyde spheres were used for the pH-controlled precipitation. The PS spheres were originally negatively charged and were used as is while the MF spheres were premodified with a monolayer of negatively charged PSS. A pH of 9 was found to be optimal for the complete precipitation of all CdTe NCs present in the solution. Confocal microscopy images of the CdTe-modified PS and MF spheres (Figure 4) demonstrate the efficient coverage and the luminescence properties of the core-shell composites formed.

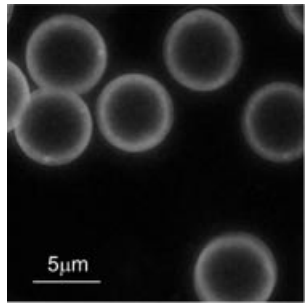

Figure 4. Confocal microscopy image of the luminescent CdTe nanocrystal shells assembled by the solvent controlled precipitation on 5 μm diameter melamine formaldehyde (MF) spheres. Reproduced from ref.[34]

Covalent Coupling of SC NCs

Interparticle Linking

Besides electrostatic coupling of NCs the generation of covalent bonds between selected nanocrystalline entities constitutes a very attractive and vast field. As an example of bridging two different sorts of NCs, we investigated the linkage of CdTe nanocrystals stabilized by TGA and MA.[35] The coupling has been carried out directly at the ligands without using an additional bridging molecule but with the aid of a carbodiimide acting as a mediator for the reaction. The reaction is described in Scheme 1. All solutions used were Ar saturated. The aqueous colloidal solution of TGA-stabilized nanocrystals (ca. 10^{-3} M according to the Cd^{2+} concentration) has been buffered to pH 5.75 by phosphate buffer and mixed with a freshly prepared solution of *N*-cyclohexyl-*N*′-[2-(*N*-methylmorpholino)ethyl]carbodiimide-4 in phosphate buffer (pH 5). After 5 min of stirring the solution was centrifuged and the precipitate redissolved in borate buffer (pH 8.65) using an ultrasonic bath. An aqueous colloidal solution of MA-stabilized nanocrystals (ca. 10^{-3} M according to the Cd^{2+} concentration) has been added and stirred for a further 90 min. While stirring the solution becomes turbid and the assembled CdTe nanocrystals precipitate. A mixture of the CdTe nanocrystal solutions without the addition of carbodiimide, and with the same buffer solutions, was used as a control experiment. In both cases the molar ratio between the different nanocrystals was approximately 1:1. The mixed nanoparticles stabilized with TGA and MA also precipitate because of electrostatic interactions.

The absorption and emission spectra of the linked and mixed nanocrystals were almost identical indicating that no obvious electronic interaction between the different nanocrystal cores seems to occur. Investigations using IR spectroscopy have been carried out in order to prove the assumption of the formation of an amide bond between the MA- and TGA-stabilized nanoparticles. The most pronounced IR absorption bands of the pure CdTe nanocrystals occur at 3500–3000 cm^{-1}, ν(OH, H_2O); 2950 cm^{-1}, $\nu(CH_2)$; 1590 cm^{-1}, $\nu_{as}(COO^-)$; 1450 cm^{-1}, $\nu_s(COO^-)$; and 1400 cm^{-1}, (δ OH) for the TGA-stabilized nanoparticles and at 3460 cm^{-1}, $\nu_{as}(NH_2)$; 3250 cm^{-1}, $\nu_s(NH_2)$; 2800 cm^{-1}, $\nu(CH_2)$; 1600 cm^{-1} (δ NH_3^+); 1490 cm^{-1}, (δ NH_3^+); and 1110 cm^{-1}, ν(CN) for the MA-stabilized nanoparticles. The IR spectra of the MA-stabilized nanocrystals show IR absorption bands that belong to both amine and protonated amine groups, indicating their coexistence on the nanocrystal surface. In the IR spectra of both nanocrystals the S–H

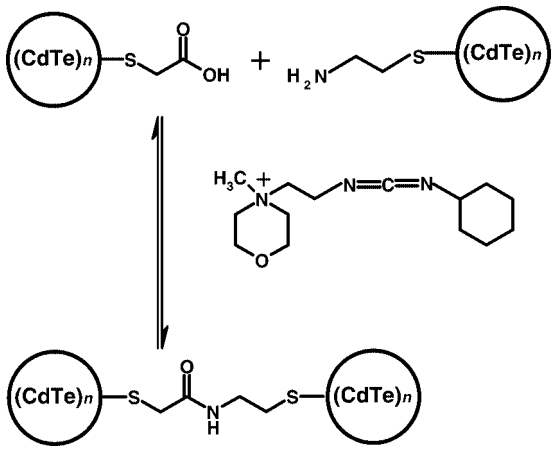

Scheme 1. Principal reaction scheme of the formation of amide bonds between differently stabilized CdTe nanocrystals. Reproduced from ref.[35] with permission of the PCCP Owner Societies.

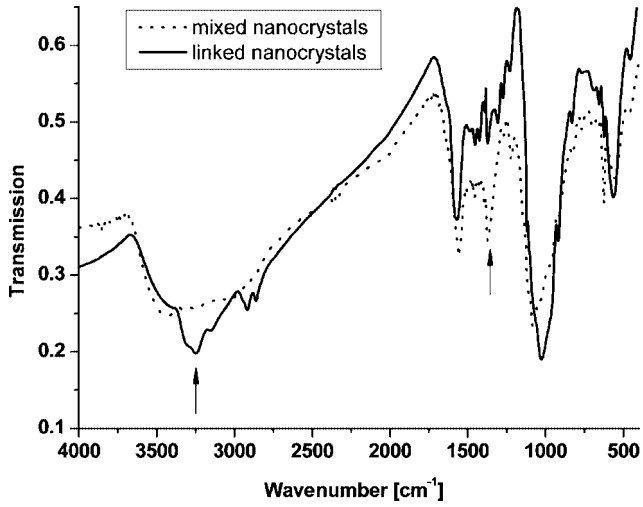

Figure 5. Infrared transmission spectra of mixed and linked CdTe nanocrystals. Reproduced from ref.[35] with permission of the PCCP Owner Societies.

vibrations (ca. 2580 cm^{-1}) are undetectable as is assumed for covalently bound thiols to the nanocrystal surface.

Figure 5 shows the IR spectra of the linked (solid line) and mixed (dotted line) nanocrystals. The main differences between the spectra in Figure 5 are marked with arrows. The IR absorption bands belonging to the valence vibrations of the carboxyl group [1550 cm^{-1}, $\nu_{as}(COO^-)$; 1370 cm^{-1}, $\nu_s(COO^-)$] are red shifted relative to the pure TGA-stabilized nanocrystals because the counterion has been changed. Whereas the spectra of the mixed nanocrystals show a broad band around 3200 cm^{-1} [ν(OH), $\nu(H_2O)$ and $\nu(NH_3^+)$] the band at 3250 cm^{-1} {ν[NH (CONH)]} in the spectra of the linked nanocrystals indicates the existence of an amide bond. Shoulders at this band indicate that some ligands remain unreacted; this is assumed to be because of steric hindrances. In the spectra of the linked nanocrystals the intensity ratio between the two bands belonging to the stretching modes of the carboxyl group has changed when compared to the spectra of the mixed nanocrystals. This is to be expected if a part of the TGA ligands have reacted with the MA. Characteristic amide group vibrations in the fingerprint region cannot be detected because of superimposition with other normal modes. The amide I band (ca. 1650 cm^{-1}), especially, is only indicated as a shoulder in the strong carboxyl group stretching band. The strong absorption bands at 1100 cm^{-1} in both spectra mainly belong to adsorbed phosphate groups originating from the buffer solutions.

Covalent Linking of CdTe NCs to Flat Surfaces

While the covalent coupling of SC NCs is still in infant status the acting chemistry as described in the preceding paragraph may well be applied to the coupling of NCs to pretreated surfaces. Accordingly, we used appropriate fractions of CdTe NCs for the conjugation with various substrates like glass, silica or silicon with different shapes of the surfaces.[36] A general illustration of the binding of the acid-stabilized NCs to aminated surfaces with the aid of carbodiimide as a mediator in the formation of the amide bond is shown in Figure 6 (inset).

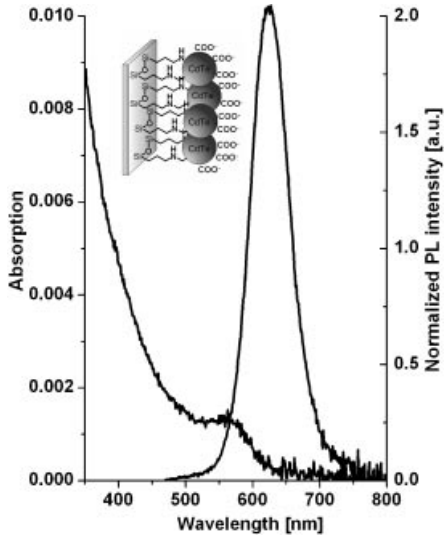

Figure 6. Absorption and luminescence spectra of CdTe NCs conjugated with a flat glass substrate. Excitation wavelength 450 nm. The inset shows a schematic representation of the structure.

The silicon wafers, quartz and glass slides were pretreated before conjugation in the following manner: the glass and quartz slides as well as the silicon wafers (with a 400 nm SiO_2 layer) were cleaned by sonication, first in 0.1 M NaOH solution, then in methanol, and finally in pure water for 15 min each. To form an amino-terminated layer on their surface, the substrates were immersed in a 6 vol.-% solution of 3-(aminopropyl)triethoxysilane in 95% methanol (named below as "3APTES solution") under sonication for 15 min followed by thorough rinsing with methanol. Drying was performed by a thermal treatment at 120 °C for half an hour in an oven.

The details of the linking of the CdTe NCs to flat substrates are as follows. An appropriate amount (0.1–0.5 mL)

of an aqueous solution of CdTe NCs was mixed with 0.5 mL of MES buffer [2-(*N*-morpholino)ethanesulfonic acid 0,1 mM] and 8 mL of Milli-Q water. The preliminarily cleaned aminated substrate was dipped into this solution. Subsequently, 0.5 mL of a solution of 1-Ethyl-3-[3-(dimethylamino)propyl]carbodiimide hydrochloride 0.025 M and *N*-hydroxysuccinimide 0.025 M (named below as "EDC/NHS solution") was added under vigorous stirring which was continued for another 10 min. After conjugation, the slides were washed three times in Milli-Q water and rinsed thoroughly in acetone and toluene and dried under vacuum conditions. Figure 6 shows optical spectra of the modified slides. The PL properties of the films prepared were found to be at least one order of magnitude more stable in time as compared to analogously LbL-assembled monolayer films. Although the surface coverage estimated from the optical densities of the modified glass slides is roughly 100% (i.e. one monolayer), the formation of islandlike multilayers could not be excluded.[9]

Covalent Linking of CdTe NCs to Spherical Surfaces

The method described is not limited to flat substrates but is of more generality, as seen by our successful attempts to coat glass spheres of micron size by CdTe NCs.[36] A dispersion (5 wt.-% in 10% solution of ethanol in water) of borosilicate glass microspheres (2 ± 0.5 μm, Duke Sci. Co., USA) was treated with 0.1 M NaOH for 15 min under sonication and washed three times in methanol by centrifugation. The treated microspheres were immersed in the 3APTES solution under sonication for 15 min and washed thoroughly with methanol by centrifugation. The final methanol dispersion was heated to boiling point for 1 h. After that, the microspheres were separated from the methanol, redispersed in 0.5 mL of MES buffer and subsequently 0.1 mL of an aqueous solution of CdTe NCs and 0.5 mL of the EDC/NHS solution was added to the dispersion under vigorous shaking which was continued for another 10 min. The conjugation was terminated by the addition of an excess amount of 0.1 M glycine solution. The spheres were washed three times with Milli-Q water and stored in an appropriate solvent, like water or DMF. In Figure 7 we display a fluorescence microscopy image of the glass spheres conjugated with the CdTe NCs. The persistency of the luminescence of the NCs is nicely seen. This luminescence is not altered for at least 3 months. The inset shows a SEM image of one particle of the same sample providing an impression of the coverage of the spheres with nanoparticles.

Figure 8 shows some optical properties of conjugates of CdTe NCs with silica beads. For the generation of these conjugates we used CdTe NCs of two different sizes, namely 3–4 nm in diameter and 6–8 nm in diameter, respectively. The absorption spectra of the conjugates possess well-pronounced first electronic transitions and strong emissions. The position of the absorption and luminescence maxima relate well to the sizes of the NCs in agreement with the size quantization effect operative in semiconductor nanoparticles of such sizes. It is seen that the emission of the larger particles reaches into the near-IR spectral region and that absorption spectra of monolayers of NCs have been gained in this study.

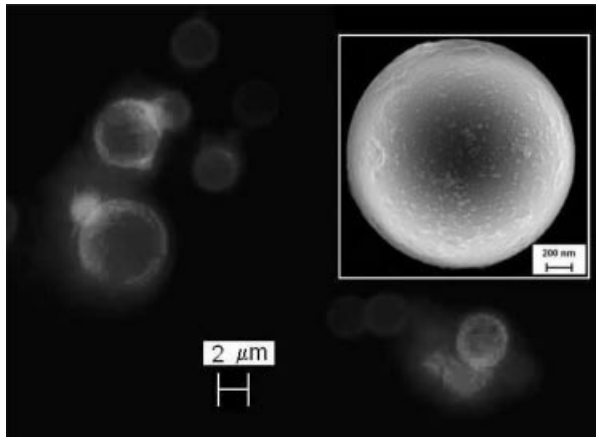

Figure 7. Fluorescence microscopy image of glass spheres conjugated with CdTe NCs. The inset shows a SEM image of one of those particles. Reproduced from ref.[36]

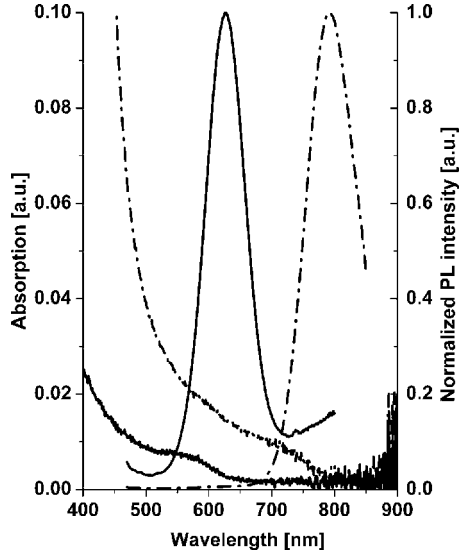

Figure 8. Absorption and luminescence spectra of silica particles conjugated with CdTe NCs of two different sizes. Reproduced from ref.[36]

For the preparation of the silica beads we used a well-known literature method.[37] Tetraethyl orthosilicate (1.5 ml) was added to a solution of ammonium hydroxide (2 mL) in ethanol (50 mL) in order to prepare particles at around 100 nm. The reaction mixture was stirred for 24 h to yield silica nanoparticles. The amino functionalization of the particles' surface was accomplished by the addition of 25 μL of 3APTES to the reaction mixture and continuing stirring for an additional 24 h. After this, the mixture was heated to boiling point for 1 h. The cooled mixture was washed three times with ethanol by centrifugation to give a stable dispersion of amino-functionalized silica spheres. Before conjugation, the silica particles were transferred into

DMF by consecutive centrifugation with the addition of fresh portions of DMF.

Conjugates of CdTe NCs with aminated silica beads have been prepared as follows. 0.05 mL of aqueous solutions of the CdTe NCs and 0.25 mL of the dispersion of the aminated silica particles in DMF were added to 0.70 mL of DMF. Then, 0.5 mL of the EDC/NHS solution (in DMF) was added with vigorous shaking. The shaking was continued for another 5–20 min. The conjugation was stopped by centrifugation of the silica particles. The conjugated silica particles were washed three times with pure DMF and stored as dispersions in the dark.

Dipole–Dipole Interactions in Layers of Nanocrystals

As described above, various methods of assembling, arranging and coupling of SC NCs have been explored but still only little is known about the properties of the solids evolving from these procedures. Some work has been published by Heath et al. on collective properties of interacting metal nanoparticles.[38,39] Depending on the interparticle distance, those solids reflect dipole–dipole interactions followed by pure electronic coupling when the particles come into closest contact. Later, Remacle and Levine performed theoretical studies on electron-transfer processes with arrays of quantum dots.[40] A shift of the first electronic absorption of small cadmium sulfide clusters to lower energies compared to their solutions was first published by Voßmeyer et al.[41] for closely packed layers of cadmium sulfide nanocrystals. The layers were built up from solutions of the clusters by a spin-coating technique and were examined by absorption spectroscopy. Besides some further studies on Förster energy transfer in semiconductor quantum solids consisting of particles of different sizes[24,42] little is known about the interaction between identical semiconductor nanoparticles. For this purpose cluster crystals are ideal candidates.

For our first studies we chose the cluster crystal compound $Cd_{17}S_4(SCH_2CH_2OH)_{26}$, which had been prepared according to the literature.[3] The structure of this thiol-stabilized molecular-like cadmium sulfide nanocrystal is known from single-crystal X-ray diffraction studies. In Figure 9 the internal structure of the cluster is shown.[3,43] It represents a tetrahedral cut out from the bulk cubic structure consisting of four adamantane-like cages capped with barrelane-like cages at the four tips of the tetrahedron. This tetrahedron has an edge length of 1.4 nm. It is also seen from Figure 9 that neighboring clusters are bound covalently via a bridging sulfur atom from the ligand at each tip of the tetrahedra. A 3D network is formed in this manner in a cubic diamondlike superstructure. Single crystals with sizes in the millimeter range are obtained via this preparation route. Because of absorption coefficients of the clusters as high as 84 000 $L\,mol^{-1}\,cm^{-1}$ it is not possible to perform absorption spectroscopy on these kinds of solids. Consequently, absorption spectra of compact layers created by spin coating of concentrated solutions of the dissolved cluster material were recorded. Figure 10 shows these spectra in comparison with a spectrum of the corresponding cluster solution of $Cd_{17}S_4(SCH_2CH_2OH)_{26}$ nanocrystals.[44] The spectrum of the compact layer recorded in transmission geometry (dashed line) was found to be shifted to lower energies in comparison to the spectrum of the cluster solution (solid line) without showing any significant broadening of the first electronic transition. Surprisingly, the absolute value of the red shift varied with the thickness of the compact layer. The maximum of the red shift in comparison to the spectra of the clusters in solution was about 70 meV at an optical density of about 0.1 at the absorption maximum. Although the compact layers appear totally transparent in the visible region a scattering background is seen in the spectra of compact layers (cf. e.g. Figure 10, dashed line). In order to avoid any measuring artifacts in the experiment an integrating sphere was used. The absorption measurement of the same layer in this different set-up resulted in significantly different signals, i.e. in the removal of the scat-

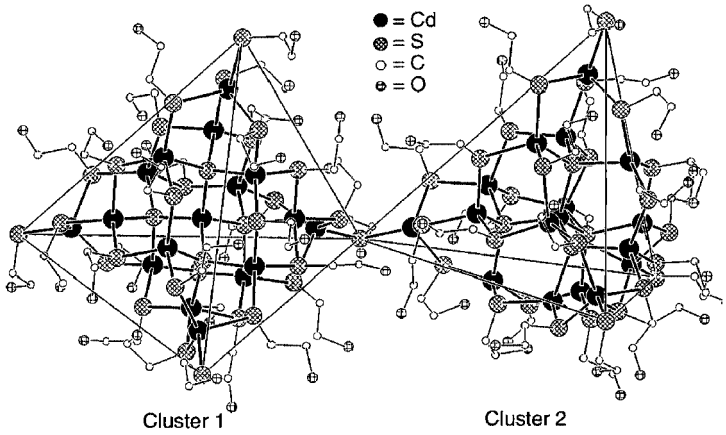

Figure 9. Crystal structure of a superstructure of $Cd_{17}S_4(SCH_2CH_2OH)_{26}$ nanocrystals. Two particles are shown that are bound covalently at the tip of each tetrahedron via a bridging sulfur atom from the ligands. For a better representation of the cores the hydrogen atoms are not shown in this Figure. Reproduced from ref.[3] with permission, copyright 1995 AAAS.

tering background (dotted line in Figure 10). Furthermore, the spectrum remains red shifted in comparison to the solution spectrum but by a smaller number than deduced before. Additionally, the measurement in the integrating sphere no longer showed a dependence on the thickness of the layers. Thus, regarding the discussion of the energetic position of an absorption band it is extremely important to suppress artifacts caused by scattering. Keeping this in mind a red shift of the first electronic transition in the compact layer of about 29 meV in comparison to the isolated cluster in solution was observed. This energy difference is taken as an indication of cluster–cluster interaction in a closely-packed layer of NCs.

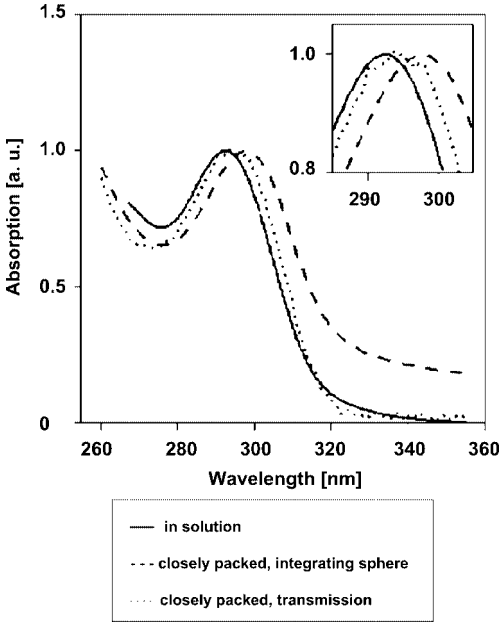

Figure 10. Absorption spectra of a compact layer of $Cd_{17}S_4(SCH_2CH_2OH)_{26}$ nanoparticles in comparison to the spectrum of the same particles in solution (solid line). Significant scattering is observed when the layer is measured in transmission geometry (dashed line) instead of measuring in the integrating sphere (dotted line). The inset provides a closer look on the resulting changes in the position of the maximum of the transition band depending on the experimental setup. (solution: cell thickness: 1 cm, OD = 1.15, calculated concentration: 0.7 μmol/L, integrating sphere: OD = 0.14, calculated film thickness: 30 nm, in transmission: OD = 0.26, calculation of film thickness is difficult because of scattering background, estimated to be 25 nm). Reproduced from ref.[44] with permission, copyright 2002 American Chemical Society.

In Figure 11 the interaction between the transition dipole moment of the absorbing particle and the induced dipole moments in the neighboring particles is sketched schematically. Analogous to the additional coulomb term for the determination of the transition energy by the Brus formula,[45] this interaction lowers the original transition energy of the absorbing particle.

Using text book equations for the values of the oscillator strength, the respective transition dipole moment and the polarizability volume, a potential energy of –51.2 meV for the interaction between the dipole of the absorbing cluster

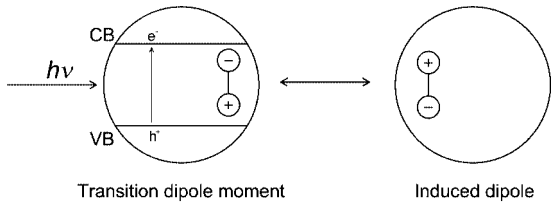

Figure 11. Schematic view of the interaction of the transition dipole moment of a particle appearing with the absorption process and the induced dipole moment of a neighboring particle. Reproduced from ref.[44] with permission, copyright 2002 American Chemical Society.

and the induced dipoles in adjacent clusters (cf. Table 1) is obtained for a distance between the particles (center to center) of 1.4 nm. It was also taken into account that for tetrahedrally shaped particles the polarizability volume decreases (57.0 Å^3), leading to a reduced shift of –14.2 meV to lower energies. Comparing these results with the value of the experiment (–29 meV), these simple calculations readily explain the red shift of the absorption band of the clusters in the compact layer in comparison to the isolated clusters in solution.

Table 1. Red shift of the first electronic transition of compact layers of CdS nanocrystals in comparison to the corresponding transition of the same clusters in solution. The experimental values for the different cluster sizes as well as the calculated results are shown. The theoretical results for both, spherically or tetrahedrally shaped particles are given. Note that for both particle sizes the experimental value fits between the values of the assumed particle shapes.

	Experimental	Calculated spherical	Calculated tetrahedral
cluster sizes	ΔE [meV]	ΔE [meV]	ΔE [meV]
d = 1.8 nm	12	27.2	6.7
d = 1.4 nm	29	51.2	14.2

Comparable results are found for the larger homologue cluster $Cd_{32}S_{14}[SCH_2CH(CH_3)OH]_{36}$ (cf. Table 1).

In an attempt to study the optical properties of the crystalline material itself, i.e. without dissolving the cluster crystals, reflection spectroscopy has been performed. For this, we milled the crystals down to grain sizes of about 2 μm and measured the diffuse reflection in an integrating sphere. In Figure 12 the UV/Vis absorption spectrum of this compound in solution is shown together with the reflection spectrum of the crystalline material. It is clearly seen that in the spectra of the crystalline material the first electronic transition is shifted to lower energies by about 150 meV, which is considerably more than observed in the films (29 meV, see above). Additionally, the transition is broadened from a full width at half maximum of about 390 meV to about 520 meV, which has not been observed in the spin-coated films consisting of the same particles. For the larger red shift a more densely packed structure of the crystals compared to the films is held responsible while for the broadening we propose a model of quantum mechanical coupling. For calculating the dependence of the electronic interaction on the distance between the coupling systems we used a periodical box potential according to Kronig and

Penney[46] for simulating both the crystalline arrangement of the particles with very small distances between them and the situation in solution with large distances between the particles. In this model, the boxes representing the particles (size 1.4 nm) are separated by potential walls. The height of these energy barriers was chosen to be 3 eV and the separation of the boxes (i.e. the interparticle distance) was varied between 20 nm, reflecting large distances, and 0.7 nm, modeling the situation with neighboring clusters. The effective masses of the charge carriers were taken from the literature (0.2 and 0.7 for electrons and holes, respectively[47]). The 3D arrangement of the particles was taken into account by multiplying the 1D results by three. According to Brus[45] the transition energy is then calculated by addition of the bulk band gap and the Coulomb interaction. For large distances between the clusters a transition energy of 3.92 eV was obtained, which is in fair agreement with the experimental value (4.24 eV). For the clusters with small distances between the inorganic cores we obtained the formation of a sub-band for the electron states, which spans about 75 meV (for 1D) for a separation of 0.7 nm. Due to the larger effective mass of the holes a narrower sub-band (1.5 meV) is observed for this charge carrier. The centers of the sub-bands remain at exactly the same energetic positions as the discrete levels in the case of the solution. Thus, it turns out that for the electronic interaction of semiconductor particles in close contact a broadening of the transition band is expected without a significant change of the transition energy. The shift of the transition energy in the crystalline material is then only due to dipole–dipole interactions of adjacent particles.

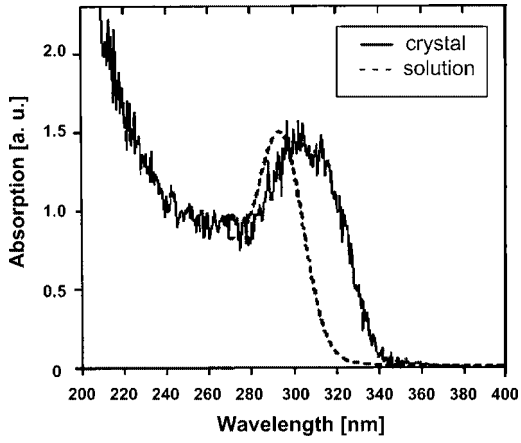

Figure 12. Absorption spectrum of $Cd_{17}S_4(SCH_2CH_2OH)_{26}$ nanocrystals dispersed in solution (dotted line) and reflection spectrum of micron-sized crystals of the same compound (solid line). Reproduced from ref.[43] with permission, copyright 2001 American Chemical Society.

Rapid Förster Energy Transfer

To investigate the Förster energy transfer from smaller (green emitting, PL maximum at approx. 555 nm) to bigger NCs (red emitting, 650 nm) in LbL-layered assemblies, two different structures both consisting of 10 polyelectrolyte/NCs bilayers have been prepared. The first structure consists of five bilayers of the same NCs size followed by five bilayers of the other NCs size on top, while the second structure consists of alternating bilayers of NCs of both sizes, as is schematically shown in Figure 13. The disappearance of the green PL band and the simultaneous relative amplification of the red emission is inherent for both structures and is a consequence of the Förster energy transfer (FRET), i.e. energy transfer takes place between donor and acceptor NCs, when the interparticle distance is smaller than the so-called Förster radius. At the same time the efficiency of the FRET appears to be relatively higher in the case of alternating layers. Indeed, the mean distance between the NCs of different sizes is smaller in the case of the alternating structure. In the other case only the closest red and green NC layers participate in the energy transfer efficiently, while others are too far apart. Furthermore, the applicability of the LbL method to the creation of even more complex structures has been demonstrated. This structure consisted of alternating bilayers of NCs of three different sizes with a gradual decrease of the electronic band gap and it shows PL originating from the biggest NCs only, while the features corresponding to all the NCs' sizes appear in the absorption spectrum (not shown here).

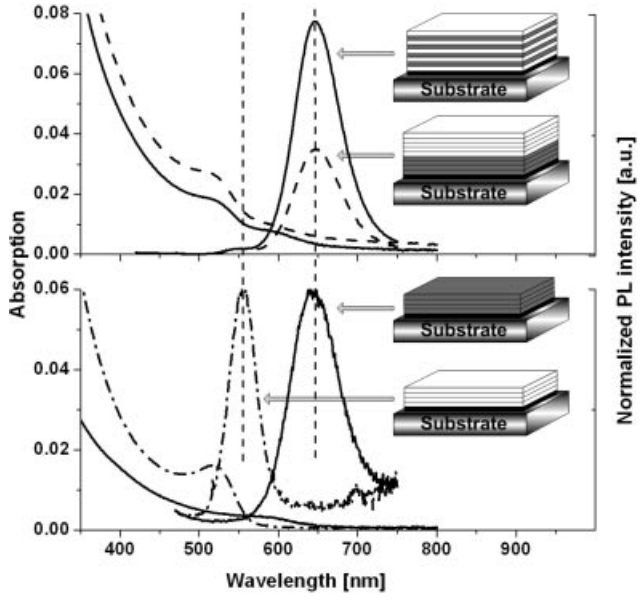

Figure 13. Absorption and PL spectra of the LbL formed assemblies sketched on the right hand side. Green and red layers correspond to the emission color of the particles constituting the assembled PE/NCs bilayers.

The FRET efficiency for thin alternating films of NCs of 2.4 and 3.5 nm in size with PDDA as opposite polyelectrolyte was estimated to be as high as 50% with an average interlayer energy-transfer rate of $(254\ ps)^{-1}$ reaching the value of $(134\ ps)^{-1}$ for certain subspecies in the inhomogeneous distribution of the donor NCs having larger spectral overlap with the acceptor NCs.[48]

As described above a LbL composite can be prepared with NCs as building blocks only, i.e. without polyelectrolytes in between the NC layers. These structures have been made in order to study Förster energy transfer in nanocrystal solids, assuming that the FRET will be facilitated by a smaller mean interlayer distance. The bilayer structure is supposed to be composed of MA-capped CdTe NCs (donors) in the bottom layer and TGA-capped CdTe NCs (acceptors) in the top layer (Figure 2). For comparison, two monolayer samples comprising only donors (MEA-capped CdTe NCs) or only acceptors (TGA-capped CdTe NCs) are also deposited on the polymer under layer. For both NC sizes the electronic transitions can be distinguished in the absorption spectrum of the bilayer sample, although the contribution of the acceptor NCs is reduced in comparison to the monolayer sample. This is not surprising because the bottom layer of the donor NCs is deposited on a polymer under layer in both cases, favoring the attachment of the NCs, while the top layer of acceptor NCs in the bilayer sample is deposited onto a preformed donor NC layer, which is apparently limited in its ability to attract and accommodate oppositely charged NCs in comparison to a polymer under layer. This is indicated schematically by an incomplete layer of acceptor NCs in the inset of Figure 2. The use of electric-field directed layer-by-layer assembly (EFDLA),[49] which relies on the additional attraction of NCs by applying an electric field to the substrate may allow this problem to be overcome. The absorption spectrum of the bilayer sample can be reproduced by a linear superposition of 1.0× the donor and 0.33× the acceptor absorption spectra. PL spectra show that almost all of the emission from the bilayer sample originates from the acceptor NCs, while the contribution from the donor NCs is strongly diminished. From the quenching of the donor and the enhancement of the acceptor NC PL in the bilayer sample, the efficiency of energy transfer in the bilayer structure is estimated to be ≈80%.

In order to determine the energy-transfer rate, we analyzed streak camera data binned by wavelengths rather than time. Figure 14 compares the PL decay of the donor NCs in the bilayer sample with the PL decay of the donor NCs in the monolayer sample at the same wavelength. To ensure that the donor decay in the bilayer sample is not affected by PL cross-talk from the acceptor NCs we chose a wavelength-binning region of interest from 500 nm to 525 nm. For both samples the PL transients appear as nonexponential decays as is typical for thiol-capped CdTe NCs.[48,50] Nevertheless, one can deduce a *1/e* decay time which decreases from 286 ps for the monolayer sample down to 57 ps for the bilayer sample. A transfer rate of $(71\ \text{ps})^{-1}$ is calculated from these numbers which is 3.5 times higher than the average transfer rate reported before for a CdTe NC bilayer structure with a polymer linker between the layers.[48] If one chooses the wavelength-binning region of interest as being more shifted to the high energy side of the donor spectrum (from 475 to 500 nm), an energy transfer time as low as 50 ps is derived, which is very close to the energy transfer rates of $(38\ \text{ps})^{-1}$ predicted by Klimov et al.[51] We attribute this increase in the energy transfer rate to the reduced average distance between the NC layers by eliminating a polymer linker in between. From the decay times provided above we derive an energy transfer efficiency of 80%, consistent with the efficiency we have calculated from time integrated PL spectra.

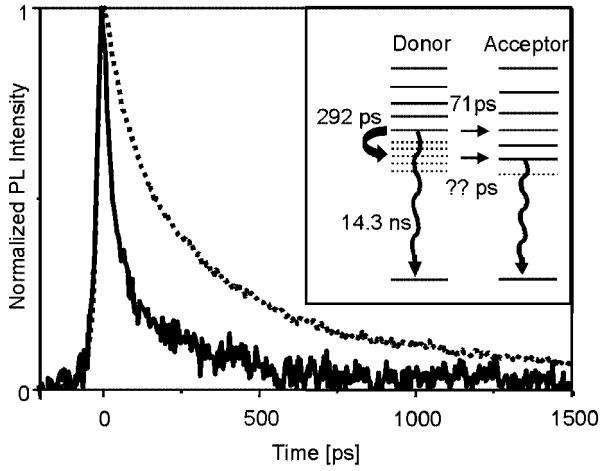

Figure 14. Fluorescence decays of the donor NCs in the monolayer donor sample (dotted line) and the donor NCs in the bilayer sample (solid line). In both samples the PL is integrated from 500 to 525 nm. The *1/e* times are 286 ps and 57 ps, respectively. The inset sketches the different decay channels of an exciton in a NC of the donor layer including the corresponding timescales. Thick solid lines represent the first excitonic transition, thin lines represent vibronic progressions and dashed lines indicate trap states from where the excitons decay nonradiatively. Apart from a resonant energy transfer of excitons in donor NC ground states, a recycling of trapped excitons by resonant transfer to a radiating state in an acceptor NC is also possible on an unknown time-scale. Reproduced from ref.[19]

Acknowledgments

Over the years contributions to this work have been made by Kathrin Hoppe, Joanna Kolny, Herwig Döllefeld, Ekkehard Geidel, Thomas Franzl, Thomas Klar, Dmitri Koktysh, Igor Radtchenko, Gleb Sukhorukov, Andrey Rogach, Jochen Feldmann, and Horst Weller. Their effort is equally appreciated as is the financial support of the DFG and the superior management of the Schwerpunktprogramm by Dr. K.-H. Schmidt and Prof. G. Schmid.

[1] C. P. Collier, T. Vossmeyer, J. R. Heath, *Annu. Rev. Phys. Chem.* **1998**, *49*, 371–404.
[2] C. B. Murray, C. R. Kagan, M. G. Bawendi, *Annu. Rev. Mater. Sci.* **2000**, *30*, 545–610.
[3] T. Vossmeyer, G. Reck, L. Katsikas, E. T. K. Haupt, B. Schulz, H. Weller, *Science* **1995**, *267*, 1476–1479.
[4] D. V. Talapin, E. V. Shevchenko, A. Kornowski, N. Gaponik, M. Haase, A. L. Rogach, H. Weller, *Adv. Mater.* **2001**, *13*, 1868–1871.
[5] A. L. Rogach, D. V. Talapin, E. V. Shevchenko, A. Kornowski, M. Haase, H. Weller, *Adv. Funct. Mater.* **2002**, *12*, 653–664.
[6] A. N. Shipway, E. Katz, I. Willner, *ChemPhysChem* **2000**, *1*, 18–52.
[7] X. Michalet, F. F. Pinaud, L. A. Bentolila, J. M. Tsay, S. Doose, J. J. Li, G. Sundaresan, A. M. Wu, S. S. Gambhir, S. Weiss, *Science* **2005**, *307*, 538–544.

[8] G. Decher, *Science* **1997**, *277*, 1232–1237.
[9] A. L. Rogach, D. S. Koktysh, M. Harrison, N. A. Kotov, *Chem. Mater.* **2000**, *12*, 1526–1528.
[10] M. Y. Gao, C. Lesser, S. Kirstein, H. Möhwald, A. L. Rogach, H. Weller, *J. Appl. Phys.* **2000**, *87*, 2297–2302.
[11] A. S. Susha, F. Caruso, A. L. Rogach, G. B. Sukhorukov, A. Kornowski, H. Möhwald, M. Giersig, A. Eychmüller, H. Weller, *Colloid Surf. A-Physicochem. Eng. Asp.* **2000**, *163*, 39–44.
[12] M. T. Crisp, N. A. Kotov, *Nano Lett.* **2003**, *3*, 173–177.
[13] T. A. Klar, T. Franzl, A. L. Rogach, J. Feldmann, *Adv. Mater.* **2005**, *17*, 769–773.
[14] A. A. Mamedov, A. Belov, M. Giersig, N. N. Mamedova, N. A. Kotov, *J. Am. Chem. Soc.* **2001**, *123*, 7738–7739.
[15] N. Gaponik, A. Eychmüller, A. L. Rogach, V. G. Solovyev, C. M. Sotomayor Torres, S. G. Romanov, *J. Appl. Phys.* **2004**, *95*, 1029–1035.
[16] S. G. Romanov, D. N. Chigrin, C. M. Sotomayor Torres, N. Gaponik, A. Eychmüller, A. L. Rogach, *Phys. Rev. E* **2004**, *69*, 046606/1–046606/4.
[17] J. W. Ostrander, A. A. Mamedov, N. A. Kotov, *J. Am. Chem. Soc.* **2001**, *123*, 1101–1110.
[18] A. Shavel, N. Gaponik, A. Eychmüller, *J. Phys. Chem. B* **2004**, *108*, 5905–5908.
[19] T. Franzl, A. Shavel, A. L. Rogach, N. Gaponik, T. A. Klar, A. Eychmüller, J. Feldmann, *Small* **2005**, *1*, 392–395.
[20] N. Gaponik, D. V. Talapin, A. L. Rogach, K. Hoppe, E. V. Shevchenko, A. Kornowski, A. Eychmüller, H. Weller, *J. Phys. Chem. B* **2002**, *106*, 7177–7185.
[21] N. A. Kotov, in: *Multilayer Thin Films* (Eds.: G. Decher, J. B. Schlenoff), Wiley-VCH, Weinheim, **2003**, pp. 207–270.
[22] F. Caruso, R. A. Caruso, H. Möhwald, *Science* **1998**, *282*, 1111–1114.
[23] F. Caruso, *Adv. Mater.* **2001**, *13*, 11–22.
[24] C. R. Kagan, C. B. Murray, M. Nirmal, M. G. Bawendi, *Phys. Rev. Lett.* **1996**, *76*, 1517–1520.
[25] P. Olk, B. C. Buchler, V. Sandoghdar, N. Gaponik, A. Eychmüller, A. L. Rogach, *Appl. Phys. Lett.* **2004**, *84*, 4732–4734.
[26] F. Müller, S. Götzinger, N. Gaponik, H. Weller, J. Mlynek, O. Benson, *J. Phys. Chem. B.* **2004**, *108*, 14527–14534.
[27] Y. P. Rakovich, L. Yang, E. M. McCabe, J. F. Donegan, T. Perova, A. Moore, N. Gaponik, A. Rogach, *Sem. Sci. Techn.* **2003**, *18*, 914–918.
[28] Y. P. Rakovich, J. F. Donegan, N. Gaponik, A. L. Rogach, *Appl. Phys. Lett.* **2003**, *83*, 2539–2541.
[29] Y. P. Rakovich, J. F. Donegan, M. Gerlach, A. L. Bradley, T. M. Connolly, J. J. Boland, N. Gaponik, A. Rogach, *Phys. Rev. A* **2004**, *70*, 051801/1–051801/4.
[30] N. Gaponik, I. L. Radtchenko, G. B. Sukhorukov, H. Weller, A. L. Rogach, *Adv. Mater.* **2002**, *14*, 879–882.
[31] N. Gaponik, I. L. Radtchenko, M. R. Gerstenberger, Y. A. Fedutik, G. B. Sukhorukov, A. L. Rogach, *Nano Lett.* **2003**, *3*, 369–372.
[32] N. Gaponik, I. L. Radtchenko, G. B. Sukhorukov, A. L. Rogach, *Langmuir* **2004**, *20*, 1449–1452.
[33] G. B. Sukhorukov, A. L. Rogach, B. Zebli, T. Liedl, A. G. Skirtach, K. Kohler, A. A. Antipov, N. Gaponik, A. S. Susha, M. Winterhalter, W. J. Parak, *Small* **2005**, *1*, 194–200.
[34] I. L. Radtchenko, G. B. Sukhorukov, N. Gaponik, A. Kornowski, A. L. Rogach, H. Möhwald, *Adv. Mater.* **2001**, *13*, 1684–1687.
[35] K. Hoppe, E. Geidel, H. Weller, A. Eychmüller, *Phys. Chem. Chem. Phys.* **2002**, *4*, 1704–1706.
[36] A. Shavel, N. Gaponik, A. Eychmüller, *ChemPhysChem* **2005**, *6*, 449–451.
[37] A. N. Shipway, M. Lahav, R. Gabai, I. Willner, *Langmuir* **2000**, *16*, 8789–8795.
[38] C. P. Collier, R. J. Saykally, J. J. Shiang, S. E. Henrichs, J. R. Heath, *Science* **1997**, *277*, 1978–1981.
[39] G. Markovich, C. P. Collier, S. E. Henrichs, F. Remacle, R. D. Levine, J. R. Heath, *Accounts Chem. Res.* **1999**, *32*, 415–423.
[40] F. Remacle, R. D. Levine, *J. Phys. Chem. B* **2001**, *105*, 2153–2162.
[41] T. Vossmeyer, L. Katsikas, M. Giersig, I. G. Popovic, K. Diesner, A. Chemseddine, A. Eychmüller, H. Weller, *J. Phys. Chem.* **1994**, *98*, 7665–7673.
[42] C. R. Kagan, C. B. Murray, M. G. Bawendi, *Phys. Rev. B* **1996**, *54*, 8633–8643.
[43] H. Döllefeld, H. Weller, A. Eychmüller, *Nano Lett.* **2001**, *1*, 267–269.
[44] H. Döllefeld, H. Weller, A. Eychmüller, *J. Phys. Chem. B* **2002**, *106*, 5604–5608.
[45] L. E. Brus, *J. Chem. Phys.* **1984**, *80*, 4403–4409.
[46] S. Flugge, *Rechenmethoden der Quantentheorie*, 5. verbesserte Auflage, Springer-Verlag, Berlin, Germany, **1993**.
[47] Landolt-Börnstein, "Numerical Data and Functional Relationships", in: *Science and Technology, Vol. 17b, New Series, Group III*, Springer-Verlag, Berlin, **1982**.
[48] T. Franzl, D. S. Koktysh, T. A. Klar, A. L. Rogach, J. Feldmann, N. Gaponik, *Appl. Phys. Lett.* **2004**, *84*, 2904–2906.
[49] M. Gao, J. Sun, E. Dulkeith, N. Gaponik, U. Lemmer, J. Feldmann, *Langmuir* **2002**, *18*, 4098–4102.
[50] A. M. Kapitonov, A. P. Stupak, S. V. Gaponenko, E. P. Petrov, A. L. Rogach, A. Eychmüller, *J. Phys. Chem. B* **1999**, *103*, 10109–10113.
[51] S. A. Crooker, J. A. Hollingsworth, S. Tretiak, V. I. Klimov, *Phys. Rev. Lett.* **2002**, *89*, 186802/1–186802/4.

Received: April 18, 2005
Published Online: August 15, 2005

